SUPPLEMENTARY MATERIAL

Handedness manipulation of propagating antiferromagnetic magnons

Yoichi Shiota[1,2,*], Tomohiro Taniguchi[3], Daiju Hayashi[1], Hideki Narita[1], Shutaro Karube[1,2], Ryusuke Hisatomi[1,2], Takahiro Moriyama[4], and Teruo Ono[1,2]

[1] *Institute for Chemical Research, Kyoto University, Uji, Kyoto 611-0011, Japan*
[2] *Center for Spintronics Research Network, Institute for Chemical Research, Kyoto University, Uji, Kyoto 611-0011, Japan*
[3] *National Institute of Advanced Industrial Science and Technology (AIST), Research Center for Emerging Computing Technologies, Tsukuba, Ibaraki 305-8563, Japan*
[4] *Department of Materials Physics, Nagoya University, Nagoya, Aichi 464-8603, Japan*
*e-mail: shiota-y@scl.kyoto-u.ac.jp

S1 Magnetometry study

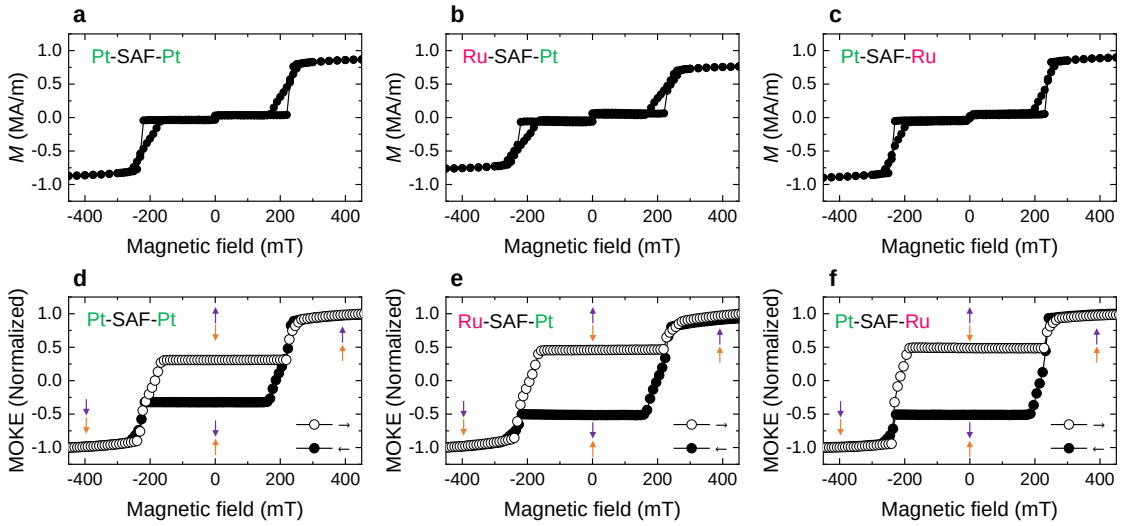

Fig. S1. a-f, Magnetic hysteresis loops under the out-of-plane magnetic field for Pt-SAF-Pt (**a,d**), Ru-SAF-Pt (**b,e**), and Pt-SAF-Ru (**c,f**) measured by SQUID magnetometer (**a-c**) and by MOKE measurement in polar configuration (**d-f**).

The magnetic hysteresis loops in the perpendicularly magnetized synthetic antiferromagnets (SAFs) were measured by using a superconducting quantum interference device (SQUID) magnetometer. Figures S1 (a-c) show the out-of-plane hysteresis loops in Pt-SAF-Pt, Ru-SAF-Pt, and Pt-SAF-Ru structures. The SAF structure consists of $[Co(0.3) / Ni(0.6)]_{8.5}$ / Ru(0.42) / $[Co(0.3) / Ni(0.6)]_{8.5}$ (thickness in nm). Both the upper and lower Co/Ni multilayers have perpendicular easy axis, and the magnetic moments between the two layers are fully compensated owing to the interlayer exchange coupling. The small changes of magnetic moments near zero magnetic field are attributed to the ferromagnetically coupled magnetic layer that exists at the edges of the substrate. Figures S1 (d-f) show the magneto-optical Kerr effect (MOKE) hysteresis loops under an out-of-plane magnetic field. Because the MOKE measurement is a surface-sensitive technique, the change in Kerr intensity associated with the magnetization reversal in the lower ferromagnetic (FM) layer is smaller than that in the upper FM layer. From this consideration, magnetization reversal of the upper FM layer occurs first in all samples as the magnetic field decreases from saturation, as depicted by purple and orange arrows. It should be noted that, unlike the magnetization curves measured by the SQUID magnetometer, there is no hysteretic behavior like ferromagnets near zero magnetic field in MOKE hysteresis loops. It indicates that there are no ferromagnetically coupled structures except for the substrate edge.

S2 Magnetic resonance study

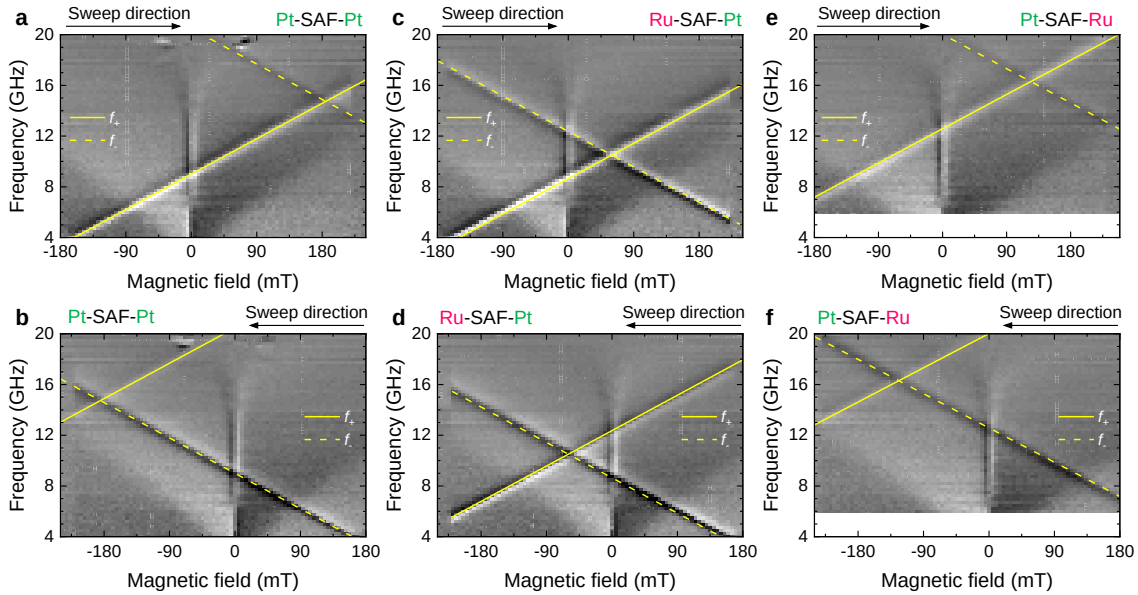

Fig. S2. a-f, Magnetic resonance spectra under the out-of-plane magnetic field in perpendicularly magnetized SAF films with various structures obtained by downward field sweep (**a,c,e**) and upward field sweep (**b,d,f**).

Table S1 Obtained parameters for perpendicularly magnetized SAF films.

Structure	$\mu_0 H_{k,1}^{\mathrm{eff}}$ [mT]	$\mu_0 H_{k,2}^{\mathrm{eff}}$ [mT]	$\mu_0 H_{\mathrm{ex}}$ [mT]
Pt-SAF-Pt	472	102	250
Ru-SAF-Pt	244	124	220
Pt-SAF-Ru	472	224	250

Field-modulated magnetic resonance spectra up to 20 GHz were measured under the out-of-plane magnetic field for Pt-SAF-Pt, Ru-SAF-Pt, and Pt-SAF-Ru structures. Each sample was placed on a coplanar waveguide, and an rf diode and lock-in amplifier were used for the measurements. The signals were recorded by sweeping the magnetic field while fixing the microwave frequency. The static magnetic field is modulated using an additional circular coil with a modulation frequency of 37 Hz. Figure S2 shows the magnetic resonance spectra under the out-of-plane magnetic field for each sample obtained by upward and downward field sweep, corresponding to tail-to-tail (T-T) and head-to-head (H-H) antiparallel magnetization configuration.

The resonance conditions for T-T and H-H antiparallel magnetization configuration are derived in Appendix B of Ref. [1] and can be expressed as

$$f_{\pm}^{\mathrm{T-T}} = \pm\frac{\mu_0\gamma}{2\pi}\left(H_{\mathrm{ext}} - \Delta H_k^{\mathrm{eff}}\right) + \frac{\mu_0\gamma}{2\pi}\sqrt{\bar{H}_k^{\mathrm{eff}}\left(\bar{H}_k^{\mathrm{eff}} + 2H_E\right)} \quad \text{(S1)}$$

$$f_{\pm}^{\mathrm{H-H}} = \pm\frac{\mu_0\gamma}{2\pi}\left(H_{\mathrm{ext}} + \Delta H_k^{\mathrm{eff}}\right) + \frac{\mu_0\gamma}{2\pi}\sqrt{\bar{H}_k^{\mathrm{eff}}\left(\bar{H}_k^{\mathrm{eff}} + 2H_E\right)} \quad \text{(S2)}$$

where $\Delta H_k^{\mathrm{eff}} = \left(H_{k,1}^{\mathrm{eff}} - H_{k,2}^{\mathrm{eff}}\right)/2$ and $\bar{H}_k^{\mathrm{eff}} = \left(H_{k,1}^{\mathrm{eff}} + H_{k,2}^{\mathrm{eff}}\right)/2$ are the difference and average of the effective perpendicular magnetic anisotropy field between upper and lower FM layers, respectively. The double sign "$\pm$" means the upper $(+)$ for right-handed (RH) precession mode and the lower $(-)$ for left-handed (LH) precession mode. The values of $H_{k,1}^{\mathrm{eff}}$ for each structure were extracted from that obtained from the magnetic resonance studies for single Co/Ni multilayer structure. The solid and dashed lines in Fig. S2 represent the resonance conditions based on Eq. (S1) and (S2). The crossing field at which the two precession modes degenerate is shifted from the zero magnetic field owing to the difference in perpendicular magnetic anisotropy between the lower and upper FM layers. In such a case, net perpendicular magnetic anisotropy field remains finite and points to the opposite direction between the H-H and T-T configurations, leading to the opposite shift of the degenerate field. The parameters to reproduce the experimental results are listed in Table S1.

S3 Device fabrication

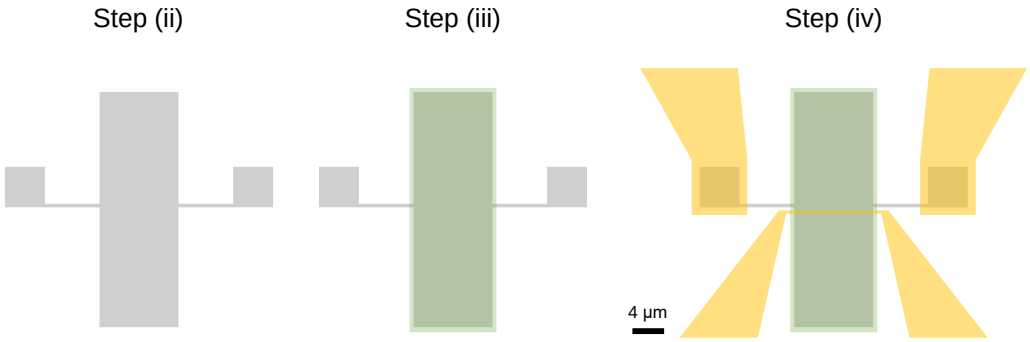

Fig. S3. Illustration of the fabrication process.

The device fabrication process mainly consists of the following 4 steps and is illustrated in Fig. S3.

(i) The global alignment marks are defined by electron-beam (EB) lithography, followed by sputtering deposition of Ti (5 nm) / Au (80 nm) and lift-off.

(ii) The Hall-bar structures with 10-μm-wide channel width and 350-nm-wide Hall probe width are defined by EB lithography and Ar ion milling process.

(iii) SiO_2 isolations are defined by EB lithography, followed by suppering deposition of SiO_2 (50 nm) and lift-off.

(iv) The contact pad for the Hall probes and microwave antennas are defined by EB lithography, followed by suppering deposition of Ti (5 nm) / Au (80 nm) and lift-off.

S4 Inverse spin Hall detection of propagating magnons in Pt-SAF-Pt structure at $\theta_H = 150°$

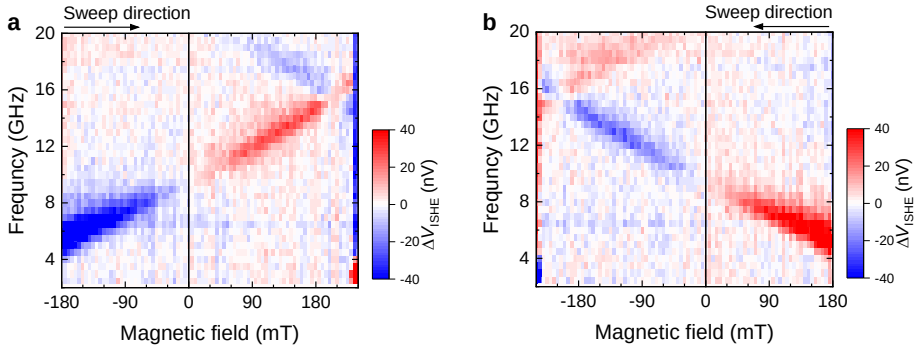

Fig. S4. a,b, ΔV_{ISHE} spectra under the tilted magnetic field $\theta_H = 150°$ for H-H antiparallel magnetization configuration (a) and T-T antiparallel magnetization configuration (b).

We also measured the inverse spin Hall detections of propagating magnons at $\theta_H = 150°$, as shown in Figs. S4 (a,b). At this field angle, the H-H antiparallel magnetization configuration becomes stable during the upward field sweep while the T-T configuration stabilized during the downward sweep, which is different from the case at $\theta_H = 30°$. It should be noted that the relationship between the magnon handedness and the sign of the ISHE voltage is the same as the results shown in Figs. 2c and 2d. Therefore, this detection method has been validated for detecting magnon handedness via the ISHE voltage.

S5 Numerical simulations of precession trajectory

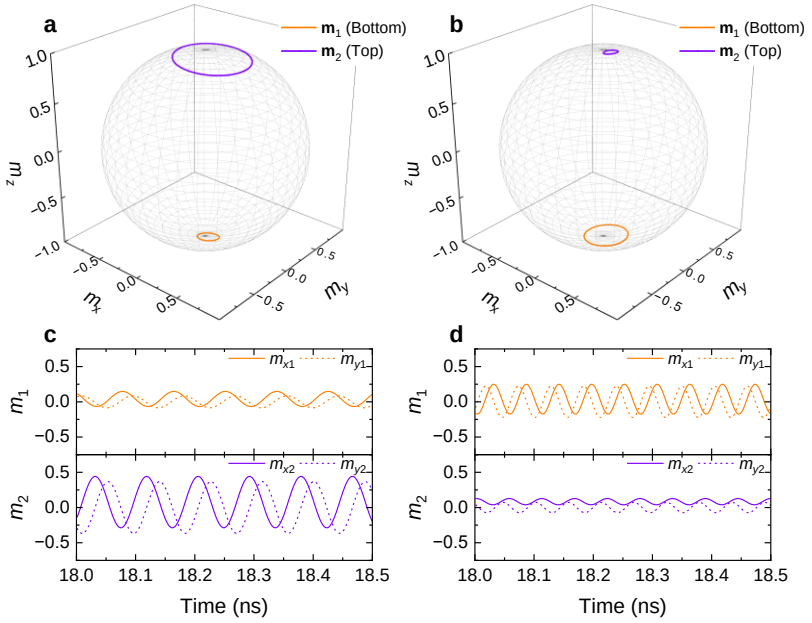

Fig. S5. a-d, Calculated magnetization trajectories and time-evolution of magnetization precession for Pt-SAF-Pt structure under external magnetic field $\mu_0 H_{\text{ext}}$ = 90 mT, θ_H = 30° with (**a,c**) f_{rf} = 11.5 GHz and (**b,d**) f_{rf} = 18.1 GHz.

We calculated the precession trajectories under fixed magnetic field of 90 mT but the different excitation frequency, as shown in Fig. S5 (a-d). Two magnetizations are set to T-T antiparallel magnetization configuration. For f_{rf} = 11.5 GHz (f_{rf} = 18.1 GHz), magnetizations in both the top and bottom FM layer have RH (LH) precession and $\mathbf{m}_2$ ($\mathbf{m}_1$) has a larger precession angle, indicating an active precession layer. Since the bottom FM layer is the active precession layer for LH mode, the visible peaks appear only for the resonance frequency of LH mode (Fig. 3a in the main text). On the other hand, the peaks for the resonance frequency of RH mode appears when the top FM layer is active (Fig. 3b in the main text). According to Eq. (1) in the main text, sign reversal of V_{ISHE} depending on the magnon handedness can be obtained when the spin Hall angles of the upper and lower HM materials are the same signs.

S6 Inverse spin Hall detection of propagating magnons in Ru-SAF-Pt and Pt-SAF-Ru structure

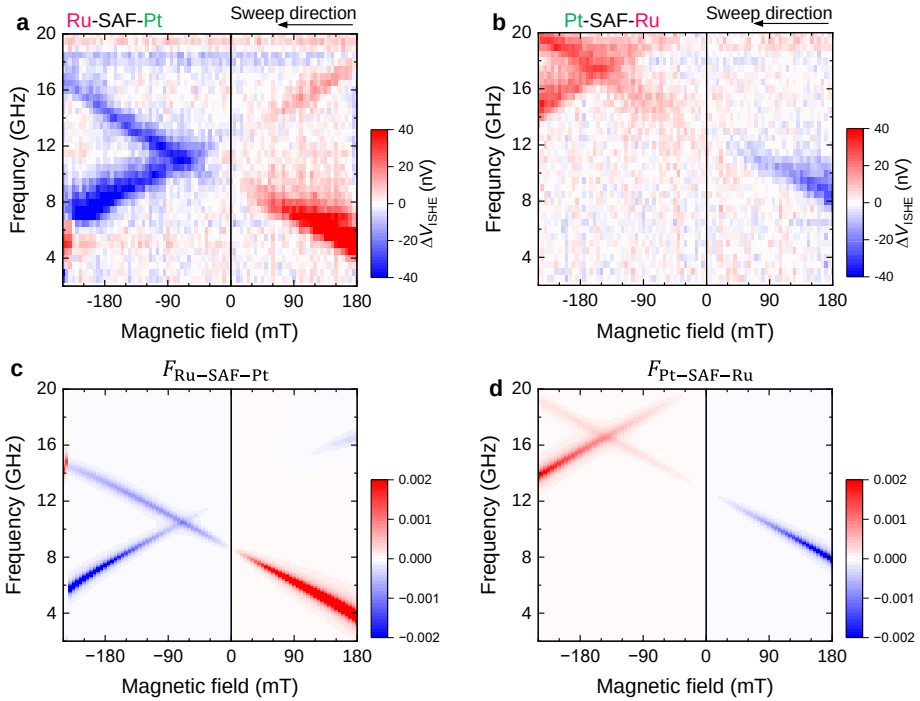

Fig. S6. a,b, Experimental results of ΔV_{ISHE} spectra under the tilted magnetic field θ_H = 30°. **c,d,** Calculated $F_{\mathrm{Pt-SAF-Ru}}$ and $F_{\mathrm{Ru-SAF-Pt}}$ spectra with Eq. (2) in the main text.

In addition to the Pt-SAF-Pt structure, inverse spin Hall detections of propagating magnons in Ru-SAF-Pt and Pt-SAF-Ru structures were also measured, as shown in Figs. S6 (a,b). Ru is chosen because it is known that the sign of the spin Hall angle is opposite to that of Pt[2], and it is a good seed layer for obtaining the perpendicular magnetic anisotropy in Co/Ni multilayers. Unlike the results for Pt-SAF-Pt structure shown in Figs. 2c and 2d in the main text, the sign of peak voltage is only inverted between the positive and negative magnetic field regions. Furthermore, the relationship between the magnetic field direction and the sign of the ΔV_{ISHE} peak differs between Ru-SAF-Pt and Pt-SAF-Ru. We also performed the numerical calculation of $F_{\mathrm{Ru-SAF-Pt}}$ and $F_{\mathrm{Pt-SAF-Ru}}$ based on Eq. (1) in the main text, which is shown in Figs. S6 (c,d). Here, the values of $\theta_{SH,\mathrm{Pt}}$ and $\theta_{SH,\mathrm{Ru}}$ are assumed to be 0.1 and -0.04, respectively[2]. The experimental results were well reproduced by simulation. These results indicate that it is difficult to distinguish the handedness of antiferromagnetic magnon if the signs of spin Hall angle between the upper and lower HMs in SAF structure are opposite.

S7 Micromagnetic simulation

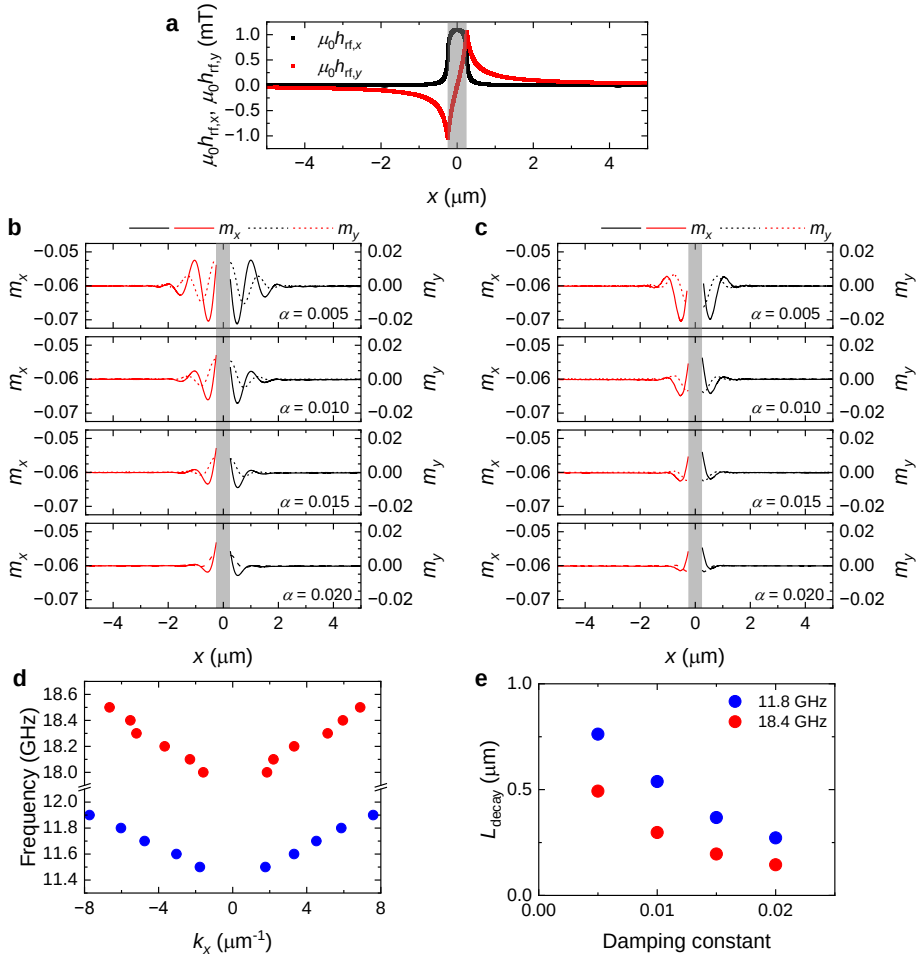

Fig. S7. a, Calculated distribution of in-plane and out-of-plane components of the microwave field used for the micromagnetic simulation. **b,c,** Snapshot images of the net magnetization m_x and $m_y$component distribution along the x-axis under external magnetic field $\mu_0 H_{\text{ext}}$ = -90 mT, θ_H = 30°, and excitation microwave frequency f_{rf} = 11.8 GHz (**b**) and 18.4 GHz (**c**), corresponding to LH mode and RH mode, respectively. Propagating magnon characteristics with various damping constant α were examined. **d,** Magnon dispersion relations for LH mode (blue circles) and RH mode (red circles). **e,** The decay length of propagating magnons L_{decay} as a function of the damping constant. Solid lines represent the calculated line as described in the text.

To reveal the propagating characteristics of antiferromagnetic magnon in SAFs, we performed micromagnetic simulation using MuMax3 code[3]. We defined the x-axis to be the magnon propagation direction, the y-axis to be the width direction of the SAF waveguide, and the z-axis to be the thickness direction. The material parameters of CoNi multilayers used in the simulation were the gyromagnetic ratio γ = 1.948 × 10^{11} rad/(Ts), the saturation magnetization M_s = 8 × 10^5 A/m, and the exchange stiffness A = 3 × 10^{-}

[11] J/m. For the Pt-SAF-Pt structure, the perpendicular magnetic anisotropy constants $K_{u,1}$ = 5.91 × 10^5 J/m^3 for the lower FM layer and $K_{u,2}$ = 4.43 × 10^5 J/m^3 for the upper FM layer were used. The nonmagnetic spacer layer was assumed to be negligibly thin, but we rescaled the exchange coupling in the region between two FM layers by the interlayer exchange energy J_{ex} = -1.5 × 10^{-3} J/m^2. The cell size used in the simulation was 5 × 5 × 7.5 nm^3. To excite the propagating magnons, we applied an alternating magnetic field in a center stripe with 500-nm-width, where the distribution of the in-plane and out-of-plane components of the microwave field, $h_{\mathrm{rf},x}$ and $h_{\mathrm{rf},z}$, was calculated using Eqs. (5) and (6) from Ref. [4] [Fig. S7 (a)]. The results were recorded at $50/f_{\mathrm{rf}}$ s after spin wave excitation.

Figures S7 (b) and (c) show snapshot images of net magnetization distribution $\mathbf{m}$ $(= (\mathbf{m}_1 + \mathbf{m}_2)/2)$ along the x-axis for different excitation frequencies. These results are fitted to an exponentially decaying sine function, and magnon dispersion relations were obtained as shown in Fig. S7 (d). The frequency in both two magnon modes increases with wavenumber k_x, indicating the positive group velocity, *i.e.* forward waves. From the slope of the dispersion relation, the group velocity v_g is evaluated to be 0.44 km/s for LH mode and 0.56 km/s for RH mode. From the result shown in Fig. S7 (e), the propagation decay length is evaluated to be 0.2 - 0.3 μm using the reasonable value of damping constant α = 0.02.

References

1. Shiota, Y., Arakawa, T., Hisatomi, R., Moriyama, T. & Ono, T. Polarization-Selective Excitation of Antiferromagnetic Resonance in Perpendicularly Magnetized Synthetic Antiferromagnets. *Phys. Rev. Appl.* **18**, 014032 (2022).
2. Liao, L. *et al.* Efficient orbital torque in polycrystalline ferromagnetic-metal/Ru/Al_2O_3 stacks: Theory and experiment. *Phys. Rev. B* **105**, 104434 (2022).
3. Vansteenkiste, A. *et al.* The design and verification of MuMax3. *AIP Adv.* **4**, 107133 (2014).
4. Chumakov, D. *et al.* Nanosecond time-scale switching of permalloy thin film elements studied by wide-field time-resolved Kerr microscopy. *Phys. Rev. B* **71**, 014410 (2005).
5. Haldar, A., Tian, C. & Adeyeye, A. O. Isotropic transmission of magnon spin information without a magnetic field. *Sci Adv* **3**, e1700638 (2017).
6. Rana, B., Fukuma, Y., Miura, K., Takahashi, H. & Otani, Y. Excitation of coherent propagating spin waves in ultrathin CoFeB film by voltage-controlled magnetic anisotropy. *Appl. Phys. Lett.* **111**, 052404 (2017).
7. Han, J., Zhang, P., Hou, J. T., Siddiqui, S. A. & Liu, L. Mutual control of coherent spin waves and magnetic domain walls in a magnonic device. *Science* **366**, 1121–1125 (2019).